Creep of sound paths in consolidated granular material detected through coda wave interferometry

David Espíndola,[1,2] Belfor Galaz,[1] and Francisco Melo[1]
[1]*Departamento de Física, Universidad de Santiago de Chile, Av. Ecuador 3493, Casilla 307, Correo 2, Santiago, Chile*
[2]*Sorbonne Universités, UPMC Université Paris 06, CNRS UMR 7190, Institut Jean Le Rond d'Alembert, F-75005 Paris, France*
(Received 3 April 2015; published 5 July 2016)

The time evolution of the contact force structure of a consolidated granular material subjected to a constant stress is monitored using the coda wave interferometry method. In addition, the nature of the aging and rejuvenation processes are investigated. These processes are interpreted in terms of affine and nonaffine structural path deformations. During the later stages of creep, the rearrangements of subgrains are so small that they only produce affine deformations in the contact paths, without any significant changes in the structural configuration. As a result, the strain path distribution follows the macroscopic strain. Conversely, in the presence of ultrasonic perturbations, the nonaffine grain buckling mechanism dominates, producing relatively drastic changes in the structural configuration accompanied by path deformations of the order of the grain size. This plastic mechanism induces material rejuvenation that is observed macroscopically as an ultrasonically accelerated creep.

DOI: 10.1103/PhysRevE.94.012901

In dense granular matter, grain movement may be extremely small relative to grain size and highly sensitive to external disturbances [1]. Although small, these subgrain rearrangements modify the structure of contacts and affect the rheological properties, such as the bulk modulus and the effective viscosity [2,3]. However, establishing the link between mesoscales and macroscales remains a challenge due to the experimental difficulties of visualization and modelization [4,5]. In this context, ultrasonic methods offer notable advantages due to high penetration and accuracy in measuring average quantities, such as sound speed and elastic constants. Furthermore, the high sensitivity of coda waves to the material microstructure allows for a characterization of structural features, such as the mean free path in both bead suspensions [6,7] and dry granular solid phase [8,9], and the detection of grain-contact rearrangements [10,11]. In addition, high-intensity ultrasound provides a mechanical disturbance that triggers and accelerates slow granular flows [12–14].

It was recently proven that the rheological properties of a granular compact evolve slowly under a constant uniaxial stress [13,15]. This creep process involves two antagonist effects: aging, which characterizes the slow internal rearrangement that brings the material to equilibrium [16,17], and rejuvenation, which accounts for the rearrangements induced by macroscopic flow renewing the internal material structure [5]. Ultrasonic disturbances were shown to strongly influence the creep process, which was characterized by the effective aging parameter [13]. This parameter decreased with the increment of ultrasonic amplitude as a consequence of material weakening and plasticity, which induced rejuvenation of the contact network structure [13,15]. The response of the strain to ultrasound was described by a generalization of the acoustic fluidization model [14,18], and it demonstrated a reduction in the effective viscosity with ultrasonic amplitude [13].

In this paper, the structural changes induced by a high ultrasonic amplitude during the creep process are investigated using the coda wave interferometry method (CWI) [19,20]. CWI uses the high sensitivity of coda waves propagating through a heterogeneous medium to characterize weak temporal perturbations induced by changes in the sound velocity, scatters position, and source placement [21]. Successful applications of CWI include the monitoring of the mechanical degradation of concrete samples [22,23], the characterization of particles or bubble suspension in liquids [19], and the variations of the relative separation between seismic sources [24]. However, to our knowledge, CWI methods have never been applied to heterogeneous granular packing. We use CWI to characterize variations in the length of the structural force chains during the creep test, considering any variation in sound speed negligible, and with the final goal of elucidating the mechanisms leading to plastic deformations in consolidated granular packing. Initially, we show that the CWI method can be used to capture the structural path distribution of strain during creep. To explain the relationship between the structural distribution of strain and macroscopic strain, a simple geometrical model is presented that considers two mechanisms of deformation: an affine (homogeneous) contact path deformation, and a nonaffine plastic deformation at the grain contact level. In the nondisturbed creep (free creep), the affine mechanism dominates and the strain path distribution is proportional to the macroscopic strain. In contrast, in the ultrasonically assisted creep (assisted creep), the ultrasound increases the nonaffine plastic events, producing drastic changes in the structural configuration.

Figure 1(a) shows the experimental setup, which consists of a cylindrical latex membrane hermetically closed by two transducers at its extremes and filled with 37 g of glass beads of mean diameter $d = 1$ mm. A cylindrical duraluminum mold, of diameter $D = 40$ mm and height $L = 20$ mm, determines the initial sample shape by evacuating the interstitial air with a vacuum pump. This process also ensures a constant hydrostatic pressure $P_o \approx 93$ kPa and a constant packing fraction $\phi \approx 0.63$. Once the mold is removed, the sample is mounted in the creep test system, where a constant uniaxial stress σ_{ext} is applied, resulting in a strain relaxation process. The longitudinal strain, γ, is measured by an inductive position sensor during which a two-cycle ultrasonic pulse of $f = 320$ kHz is sent through the sample at 200 ms intervals by a HFE transducer of 30 mm diam. The transmitted waves are received by a HFR miniature transducer of 2 mm diam positioned at the base, as shown in Fig. 1(a). A low-frequency transducer (LFE) is located at base of the sample. This

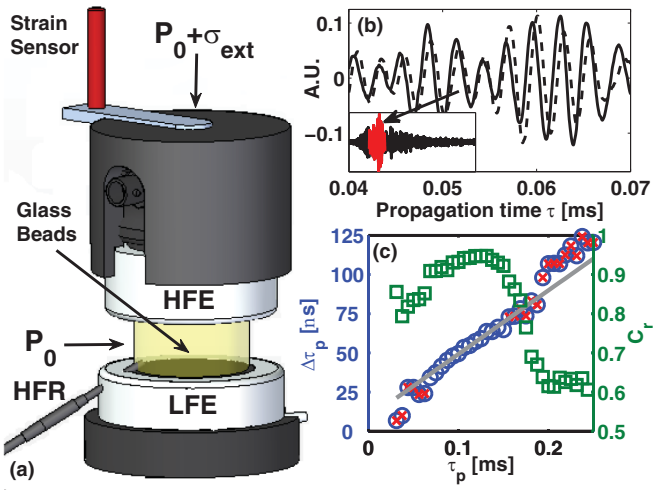

FIG. 1. (a) Experimental setup. HFE: high-frequency emitter transducer; LFE: low-frequency emitter transducer, used to disturb the packing; HFR: miniature high-frequency receptor. (b) Time shift of the signal window (red). The inset in (b) depicts a typical coda wave signal resulting from the high pass filter application. (c) Relative correlation C_r and linear fit of the time shifts (circles). Crosses indicate points eliminated by the correlation filter.

perturbs the granular packing through the transmission of a two-cycle pulse at 50 kHz every 1 s, with a delay with respect to the high-frequency pulse in order to avoid interferences. The specific advantage of this experimental setup is the independent control of longitudinal and transverse stress, improving the approach to the yield stress limit. To visualize the gradual changes induced by the low-frequency pulse on the structural contact force network, the creep is first monitored for 3 h, and then the amplitude of the perturbing pulse is increased gradually from $\epsilon_{US} = 10$ to 350 nm for 40 min (8.5 nm/min). This gradual increase of ϵ_{US} prevents excessive decorrelation between consecutive signals [Fig. 2(a)], allowing the use of the CWI method. A typical signal detected by the HFR corresponds to propagated waves in the range $\lambda \approx 2d$,

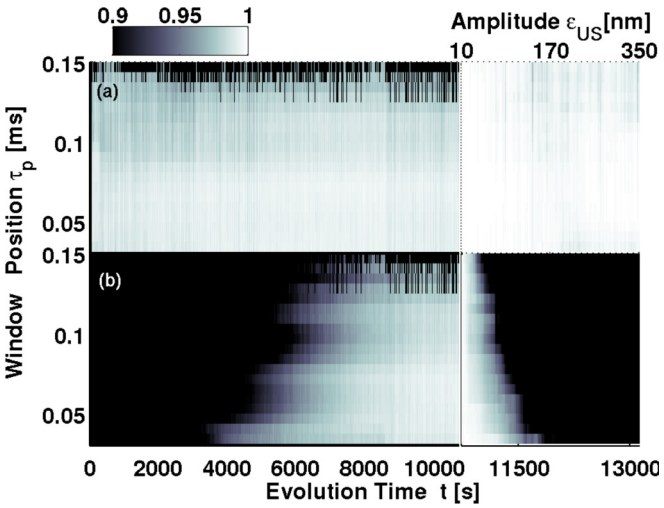

FIG. 2. Correlations for $\sigma_{ext} = 68$ kPa. (a) Relative correlation C_r. (b) Absolute correlation C_a.

where the coherent and incoherent components are present. Considering that the external pulse used to monitor the internal deformation has a narrow frequency content ranging from 280 to 400 kHz, the coherent component, which is centered at 100 kHz, is generated by the medium itself by means of a nonlinear mixing of frequencies [8,10]. On the other hand, the incoherent component of the signal is centered at the excitation frequency (320 kHz), and it corresponds to the coda waves traveling through different force chains or paths. For this reason, before applying the CWI method, the coherent component is eliminated using a high-pass frequency filter with a cutoff frequency of 200 kHz [Fig. 1(b)].

Following the CWI theory [25], the wavefield u can be written as a superposition of waves S_p that propagate along all the possible scattering paths p, i.e., $u(\tau) = \sum_p S_p(\tau)$. In a weakly perturbed sample, the new wavefield u' can be obtained by adding a time shift, $\Delta\tau_p$, which is $u'(\tau) = \sum_p S_p(\tau - \Delta\tau_p)$. The CWI method compares the waves before (u) and after (u') a small perturbation using the time-windowed correlation function $c^{(\tau,t_w)}(\tau) = \int_{\tau_p - t_w}^{\tau_p + t_w} u(\tau')u'(\tau' + \tau)d\tau'$, where t_w is the window width. For a granular packing, the induced travel-time perturbation $\Delta\tau_p$ depends of the characteristics of the scattering path p, which are dominated by mechanical properties at the contact-grain interfaces. However, with respect to acoustical propagation, $\Delta\tau_p$ can be described in terms of its characteristic length l_p and sound speed c_p, as $\tau_p = l_p/c_p$. In this context, a variation of travel time corresponds to a variation of either l_p and/or c_p. However, the variation of bulk sound speed was measured during the free creep process and was found to be negligible with respect to the macroscopic strain [13]. Later, we will validate this hypothesis by showing that during slow creep, the macroscopic strain can be reconstructed by considering a path-length variation, which induces a time-delay proportional to the window position. The variation of path lengths $\Delta l_p/l_p$ can be interpreted as the relative strain variation for the path p with average travel time τ_p, thus $\Delta\tau_p/\tau_p \approx \Delta l_p/l_p \approx \Delta\gamma_p$ [26]. The integration of the last expression over time gives an estimate of the internal strain distribution,

$$\gamma_p(t) = \int_0^t \frac{\Delta\gamma_p}{\Delta t}dt' = \int_0^t \frac{\Delta\tau_p}{\tau_p \Delta t}dt'. \quad (1)$$

Two consecutive coda waves are compared by using the time-windowed correlation coefficient, which allows the determination of $\Delta\tau_p$. First, both signals are segmented in overlapped windows of width ten times the characteristic period of the signals [Fig. 1(b)]. An overlapping factor of 90% is used to improve the statistical calculations by increasing the number of windows. Both the window width and the overlapping factor allow the central window position τ_p to be defined. The time delay $\Delta\tau_p$ is then expressed as the time location at the maximum of the relative correlation C_r. Large errors in the estimated time-delay values are eliminated using the correlation as a quality indicator [Fig. 1(c)]. This defines a region of the signals with sufficient resolution to calculate time delays.

The maximum of correlation between consecutive coda waves, C_r, is shown in Fig. 2(a). Highly correlated signals are continuously observed, and they justify the selection of

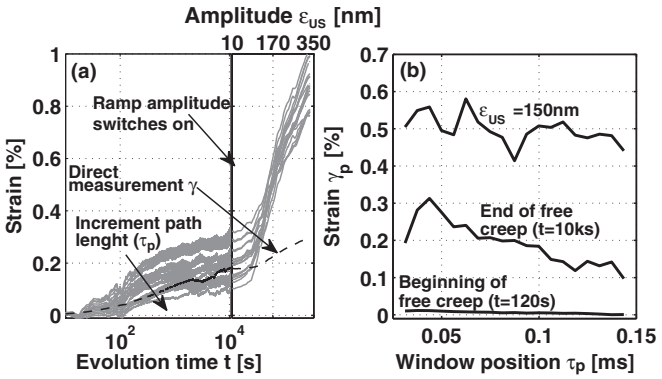

FIG. 3. (a) $\gamma_p(t)$ distribution, for $\sigma_{ext} = 68$ kPa, as a function of time for different initial paths characterized by the window position τ_p. The dashed line is the strain obtained through the inductive sensor. (b) $\gamma_p(t)$ distribution as a function of the initial path length τ_p before and during the ultrasonic perturbation.

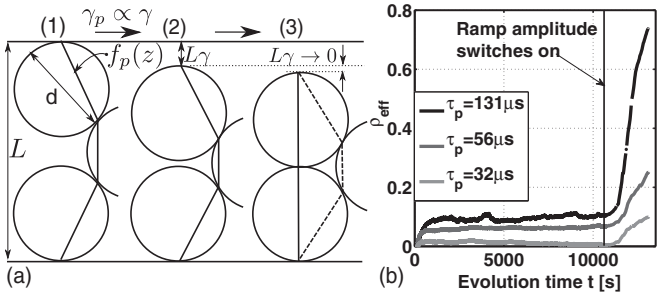

FIG. 4. (a) Diagram of an affine or nonaffine path deformation. From (1) to (2): affine. From (2) to (3): nonaffine grain ejection or insertion mechanism. The ejected grain induces a drastic change in the path length with a minimal external compression (3). (b) Density of events ρ_{eff} computed from the experimental data in Fig. 3.

the time step with the use of the CWI method. We define the absolute correlation, C_a [Fig. 2(b)], as the maximum of correlation, which is determined by using as a reference the final signal received before the initiation of the ramp of ultrasound. For the free creep, a slow and smooth evolution of the absolute correlation is visualized, which implies a process governed by small and slow rearrangements of the internal structure. However, it is noted that longer paths are more sensitive to decorrelation due to their increased probability of generating plastic events. As the ultrasonic amplitude increases, the correlation gradually decreases, having a more significant effect on the longest paths. This shows a higher sensibility to the rejuvenation that is induced by the perturbing wave. In the amplitude ramp zone, the absolute correlation abruptly decreases with ultrasonic amplitude, indicating that a higher density of plastic events affects the structural force network.

The strain distributions can be estimated using the maximum of the correlation and Eq. (1); these are shown in Fig. 3(a). The initial path length increases in the direction of the arrow. The macroscopic strain γ, represented by the dashed line, follows an almost logarithmic tendency [13,15], and each path approximately follows the shape of the macroscopic deformation. Figure 3(b) shows the deformation profiles at different stages of the creep. For the free creep, a decreasing deformation profile is observed, which means that short paths deform more than long paths. In contrast, this profile is flatter in the presence of ultrasound. In the presence of perturbations, the path deformations gradually increase with the ultrasound amplitude, and they are significantly larger than the macroscopic measured strain [Fig. 3(a)]. In general, the path strain distribution is greater than the macroscopic measured strain. This is more extreme in the perturbed zone, which reveals the presence of local deformations that are not visible on the macroscopic scale.

To obtain an overall understanding of this phenomenon, the hypothesis that the creep process is mostly governed by affine or homogeneous deformations was used as a basis. Consider an affine deformation over a general path p joining two end points of the sample along the z coordinate. In cylindrical coordinates, it is possible to estimate the shape of the path with length l_p, in a continuous approach, by the function $f_p(z)$ [Fig. 4(a)]. After a small macroscopic deformation h/L over the z direction, the length of the path becomes $l_p - \Delta l_p = \int_0^L \sqrt{(1-\gamma)^2 + f_p'(u)^2}du$, where $u = z/(1-\gamma)$. Note the assumption that path deformation predominantly occurs in the direction of the applied external stress. A Taylor series expansion leads to $\gamma_p \approx L\gamma G_p/l_p$, where $G_p = \int_0^L [1 + f_p'(u)^2]^{-1/2}du$ depends on the geometry of the path. Numerically, multiples shapes or functions for $f_p(z)$ were tested to evaluate G_p, which is found to scale as $G_p \approx L/l_p$. In this context, since the term L/l_p is less than 1, the strain path distribution γ_p should always be less than the macroscopic strain γ. However, our experimental data do not show this feature [Fig. 3(a)]. To be consistent with our experimental observations, we propose a second mechanism that considers both the lateral ejection and insertion of a grain into the chain.

Figure 4(a) shows a schematic diagram of path deformation. From (1) to (2), the deformation of the path is proportional to the deformation of its vertical projection. Conversely, from (2) to (3), the ejection mechanism causes an abrupt change in the path length that involves a slight variation of vertical distance between grains. Thus, buckling produces a slow lateral displacement that is affine, and a subsequent grain ejection that modifies the shape of the path, increasing drastically the path deformation with a negligible macroscopic effect. Geometrically, this local deformation is proportional to d/l_p, and it may be positive or negative depending on whether the grain is ejected or inserted into the chain. Since the CWI-based strain is computed using finite-size windows with a path distribution of similar length, multiple local ejection and insertion (plastic events) can be asynchronously present in each window of the signal. This final mechanism allows for the definition of an effective event probability density of grain ejection or insertion, ρ_{eff}, which leads to $\gamma_p \approx L\gamma G_p/l_p + \rho_{eff} d/l_p$. ρ_{eff} is interpreted as the shortening or enlargement of a path (relative to its initial length and due to plastic events). Thus, γ_p results from the competition between the aging (affine deformation) and rejuvenation (plastic events) mechanisms.

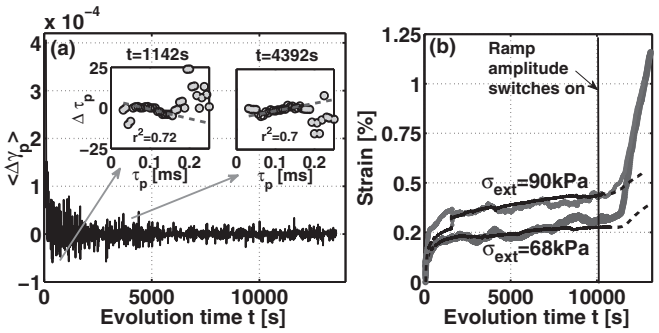

FIG. 5. (a) Slope evolution of linear fit $\langle \Delta\gamma_p \rangle = \langle \Delta\tau_p/\tau_p \rangle$ for the free creep experiment. Inset: time shift by windows $\Delta\tau_p$. The gray circles represent data disregarded due to low correlation, while the dashed red line represents the linear fit. (b) Direct measurement of the macroscopic strain (dashes lines) and CWI-based strain reconstruction for two values of σ_{ext}.

Figure 4(b) presents the probability of occurrence of plastic events ρ_{eff}, calculated from the experimental data as $\rho_{\text{eff}} \approx \gamma_p l_p/d - L^2\gamma/(l_p d)$. Results agree that more intricate paths have an increased probability of generating buckling. For example, in a path with $\tau_p = 32$ μs, only 1.5% of the total deformation after 1000 s is due to plastic events, while in a path with $\tau_p = 131$ μs this percentage increases to 9%. Furthermore, the magnitude of ρ_{eff} increases considerably with the amplitude of the ultrasonic perturbation, increasing the probability of grain slip and promoting the occurrence of plastic events. The high sensibility of the CWI method in visualizing local plastic events of lateral grain ejection or insertion justifies the overestimation of CWI-based strain with respect to the macroscopic measurement, which is solely affected by global effects.

To compare the directly measured strain and our CWI-based strain, an average strain was obtained with a suitable linear fit of $\Delta\tau_p$ against τ_p. Paths are selected to exclude all the windows with correlation coefficients below 0.9 from the fit [see the insets of Fig. 5(a)]. In this way, the slope represents the average of $\Delta\tau_p/\tau_p$ over the paths. During the creep experiment, the slope $\langle \Delta\tau_p/\tau_p \rangle = \langle \Delta\gamma_p \rangle$ shows an initial positive value that corresponds to the initial axial compression of the sample. This is followed by time-decreasing amplitude fluctuations around zero (Fig. 5). In the less favorable scenario, the fluctuations at long time scales are relate to the noise level of our measurement. However, at early stages, these fluctuations are due to instantaneous compressions and expansions of some force chains, confirming the nonaffine lateral grain ejection or insertion mechanism as previously described. The integration of this curve yields the reconstructed CWI-based macroscopic strain, which is showed in Fig. 5(b) for two different experiments with $\sigma_{\text{ext}} = 68$ and 90 kPa. The averaging process, applying the aforementioned linear fit, smoothes the local details when the number of plastic events is small, which explains the similarity between the CWI-based strain reconstruction and macroscopic strain in the free creep zone. However, in the ultrasonic perturbation zone, the frequency of plastic events increases, inducing a more intense local deformation, which is evident as the average strain is considerably higher than the macroscopic strain. In our previous work [13] and in [11], it was demonstrated that the acoustic perturbation induces a clear material rejuvenation or equivalently a sound speed decrease. However, in the presence of ultrasonic perturbation, our experiments indicate that the coda wave arrives earlier, which is inconsistent with a sound speed decrease. We are thus forced to consider that sound paths are shortened. If the sound speed decrease is considered in the CWI-reconstruction, then the path shortening would be even more pronounced in the ultrasonic perturbation zone.

In conclusion, the CWI method gives quantitative information about the distribution of strain along the complex contact paths defined by the force chains structure if the sound speed variations are small. In the present work, during the whole creep experiment, speed variations were smaller than 0.02%, which ensures a maximum error on the determination of strain distribution of 20%.

A geometric model, based on affine path deformations and nonaffine plastic events, can phenomenologically capture the features observed experimentally. The free creep is presented as a competition between the aging process, where the whole structure has similar deformation, and the rejuvenation process, where plastic events trigger local path deformations with an almost negligible presence on a macroscopic scale. In the perturbation zone, the high amplitude induces sliding of the grain contacts on a finite time scale, which increases the density of plastic events, and it is followed by an accelerated sample compression revealing contact rejuvenation. Finally, an average CWI-based strain is calculated, which describes the temporal behavior of the macroscopic sample deformation during the slow creep, validating the hypothesis of constant sound-speed across the sample.

The authors are grateful to E. Clément, J-Ch. Géminard, G. Lagubeau, and S. Job for several constructive discussions. This project was financed by ANR-Fondecyt 011 and Fondecyt 11110289 and 1130922.

[1] H. A. Makse, N. Gland, D. L. Johnson, and L. Schwartz, Phys. Rev. E **70**, 061302 (2004).
[2] P. A. Johnson and X. Jia, Nature (London) **437**, 871 (2005).
[3] A. Amon, V. B. Nguyen, A. Bruand, J. Crassous, and E. Clément, Phys. Rev. Lett. **108**, 135502 (2012).
[4] F. Lequeux and A. Ajdari, Phys. Rev. E **63**, 030502 (2001).
[5] C. Derec, A. Ajdari, and F. Lequeux, Eur. Phys. J. E **4**, 355 (2001).
[6] J. H. Page, H. P. Schriemer, A. E. Bailey, and D. A. Weitz, Phys. Rev. E **52**, 3106 (1995).
[7] R. L. Weaver and W. Sachse, J. Acoust. Soc. Am. **97**, 2094 (1995).
[8] X. Jia, Phys. Rev. Lett. **93**, 154303 (2004).
[9] S. Griffiths, A. Rescaglio, and F. Melo, Ultrasonics **50**, 139 (2010), selected papers from ICU 2009.
[10] V. Tournat and V. E. Gusev, Phys. Rev. E **80**, 011306 (2009).

[11] X. Jia, T. Brunet, and J. Laurent, Phys. Rev. E **84**, 020301 (2011).
[12] P. Lidon, N. Taberlet, and S. Manneville, Soft Matter **12**, 2315 (2016).
[13] D. Espíndola, B. Galaz, and F. Melo, Phys. Rev. Lett. **109**, 158301 (2012).
[14] H. J. Melosh, Nature (London) **379**, 601 (1996).
[15] V. B. Nguyen, T. Darnige, A. Bruand, and E. Clement, Phys. Rev. Lett. **107**, 138303 (2011).
[16] L. C. E. Struik, Ph.D. thesis, TU Delft, Delft University of Technology (1977).
[17] J. Sullivan, Compos. Sci. Technol. **39**, 207 (1990).
[18] H. J. Melosh, J. Geophys. Res. **84**, 7513 (1979).
[19] R. Snieder, A. Gret, H. Douma, and J. Scales, Science **295**, 2253 (2002).
[20] R. Snieder, Pure Appl. Geophys. **163**, 455 (2006).
[21] R. Snieder and J. Page, Phys. Today **60**(5), 49 (2007).
[22] S. C. Stähler, C. Sens-Schönfelder, and E. Niederleithinger, J. Acoust. Soc. Am. **129**, 1945 (2011).
[23] D. P. Schurr, J.-Y. Kim, K. G. Sabra, and L. J. Jacobs, NDT & E Int. **44**, 728 (2011).
[24] R. Snieder and M. Vrijlandt, J. Geophys. Res. **110**, B04301 (2005).
[25] R. Snieder and M. Hagerty, Geophys. Res. Lett. **31**, L09608 (2004).
[26] J. P. Poirier, *Creep of Crystals: High-temperature Deformation Processes in Metals, Ceramics, and Minerals*, Cambridge Earth Science Series (Cambridge University Press, Cambridge, 1985).